Electronic Supplementary Material (ESI) for Journal of Materials Chemistry A.


# Enhanced durability of Li−$O_2$ batteries employing vertically standing Ti nanowire array supported cathodes

Guangyu Zhao, Li Zhang, Yanning Niu, Kening Sun* and David Rooney

Academy of Fundamental and Interdisciplinary Sciences, Harbin Institute of Technology, Harbin 150001, (China)

E-mail: keningsunhit@126.com

## Experimental Section

*Sample Preparation.* Ti nanowire arrays were fabricated on circular Ti (Ti-Mo alloy, Mo=0.3 wt%) alloy foam plates purchased from Baiji Jinkai Corporation of China using an electroless wet chemical etching method. The etching was carried out in 0.25 wt% HF solution for different times. The obtained Ti nanowire arrays were rinsed with deionized water fully and dried overnight. Au nanoparticles were deposited on the Ti nanowire arrays by a Leica EM SC050 cool sputtering device at a current of 20 mA for 80 s. The weights of the deposits were measured by means of a micro-balance (Mettler Toledo, USA) with an accuracy of 0.01 mg. The mass of Au nanoparticels was around 1 mg $cm^{-2}$.

*Instruments for Characterization.* Scanning electron microscope (SEM) images and Energy dispersive X-ray spectroscopy (EDS) were obtained on a Hitachi Su-8100. The X-ray diffraction (XRD) patterns were obtained on a PANalytical X´pert PRO X-ray diffractometer with Cu Kα radiation ($\lambda$ = 1.5418 Å). X-ray photoelectron

spectra (XPS) were obtained with a K-Alpha electron spectrometer (Thermofish Scientific Company) using Al Kα (1486.6 eV) radiation. The base pressure was about $1\times10^{-8}$ mbar. The binding energies were referenced to the C1s line at 284.8 eV from adventitious carbon. The surface area of the materials was analyzed by the Brunauer-Emmett-Teller (BET) method with a Micromeritics Accelerated Surface Area and Porosimetry System (ASAP) 2020. The gas used was $N_2$ with a liquefaction temperature of –195.87 °C, and the gas desorption time was 6 h. Transmission electron microscope (TEM) images and selected area electro diffraction (SAED) patterns were obtained on a JEOL-2100. The cyclic voltammetry (CV) and electrochemical impedance spectroscopy (EIS) tests of the batteries were carried out on a CHI 660 electrochemical workstation. $^1$H nuclear magnetic resonance (NMR) analysis was carried on a Bruker ADVANCE III 400MHz NMR analyzer.

*Li–$O_2$ battery tests.* The Swagelok type Li–$O_2$ batteries were assembled inside an MBraun glove box. The cells were constructed by placing a 15 mm diameter Li disk on the bottom, covering it with a piece of glass fiber separator (20 mm diameter, Whatman), adding excess electrolyte (1.0 M LiTFSI in tetraethylene glycol dimethyl ether (TEGDME)), placing a Au nanoparticle modified Ti nanowire array electrode disk (15 mm diameter) on the separator, and sealing the Swagelok cell. All the electrochemical measurements to the batteries were carried out in pure $O_2$ at 1 atm (99.99%). A BTS-2000 Neware Battery Testing System was employed for charge/discharge tests.

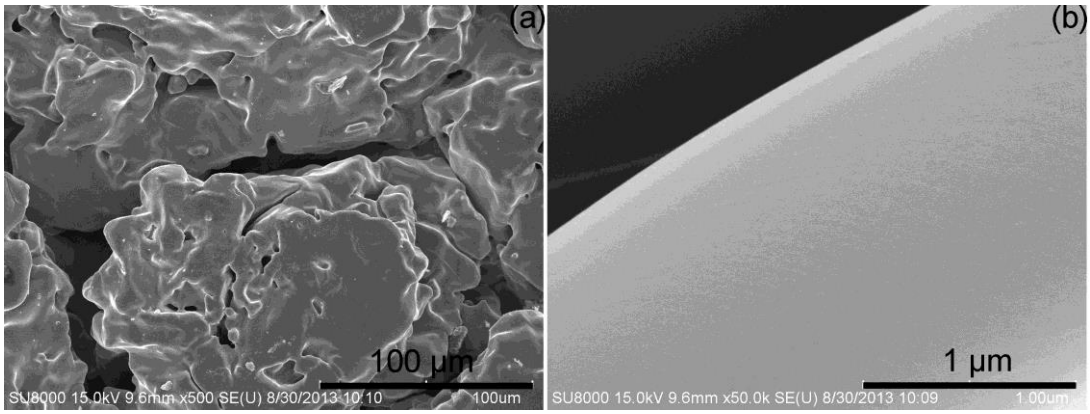


Fig. S1. SEM images of the raw Ti alloy foam.

In this it is clear that the SEM images of raw Ti alloy foam exhibit a smooth surface.

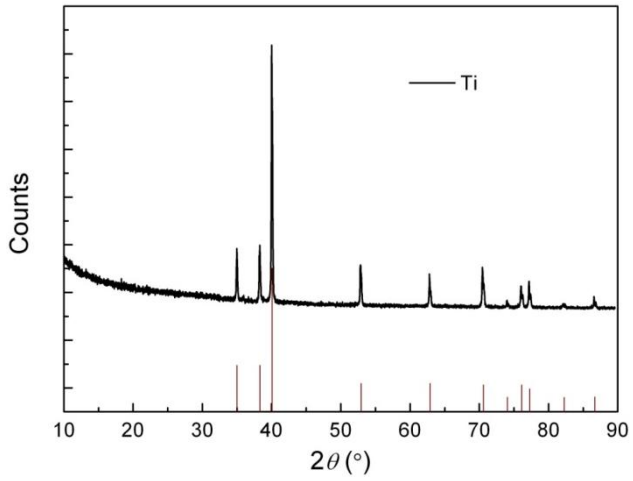


Fig. S2. XRD pattern of raw Ti alloy foam.

This pattern is ascribed to Ti metal (JCPDS: 65-9622*a*=2.951, *b*=2.951, *c*=4.686), revealing that the primary component is Ti. The low Mo content peaks are undetected in the XRD pattern.

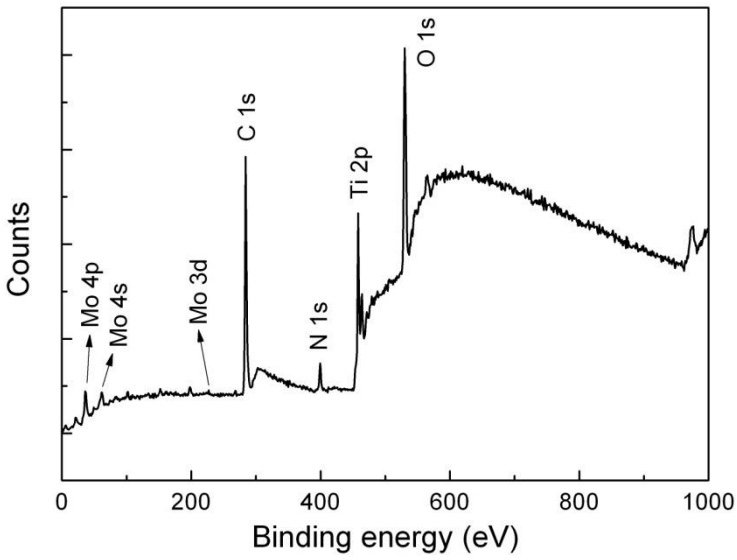


Fig. S3. XPS of raw alloy Ti foam.

This analysis however shows the existence of Mo.

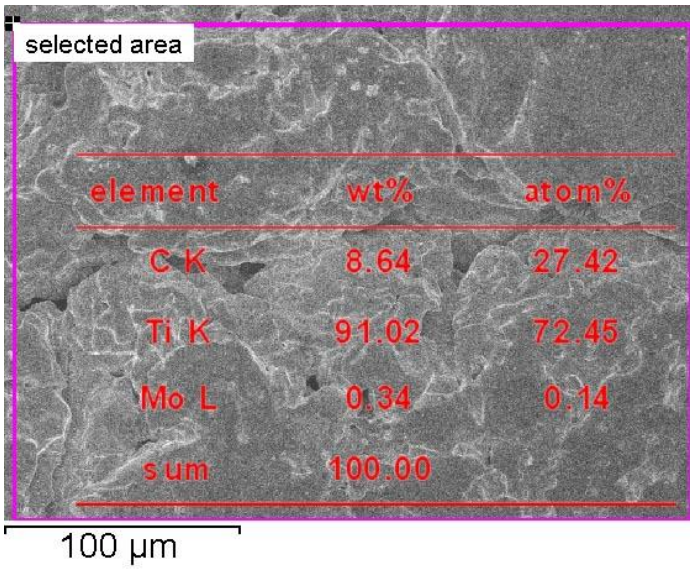


Fig. S4. EDS of raw alloy Ti foam.

Analysis of this data demonstrates that the Mo content is 0.34 wt%.

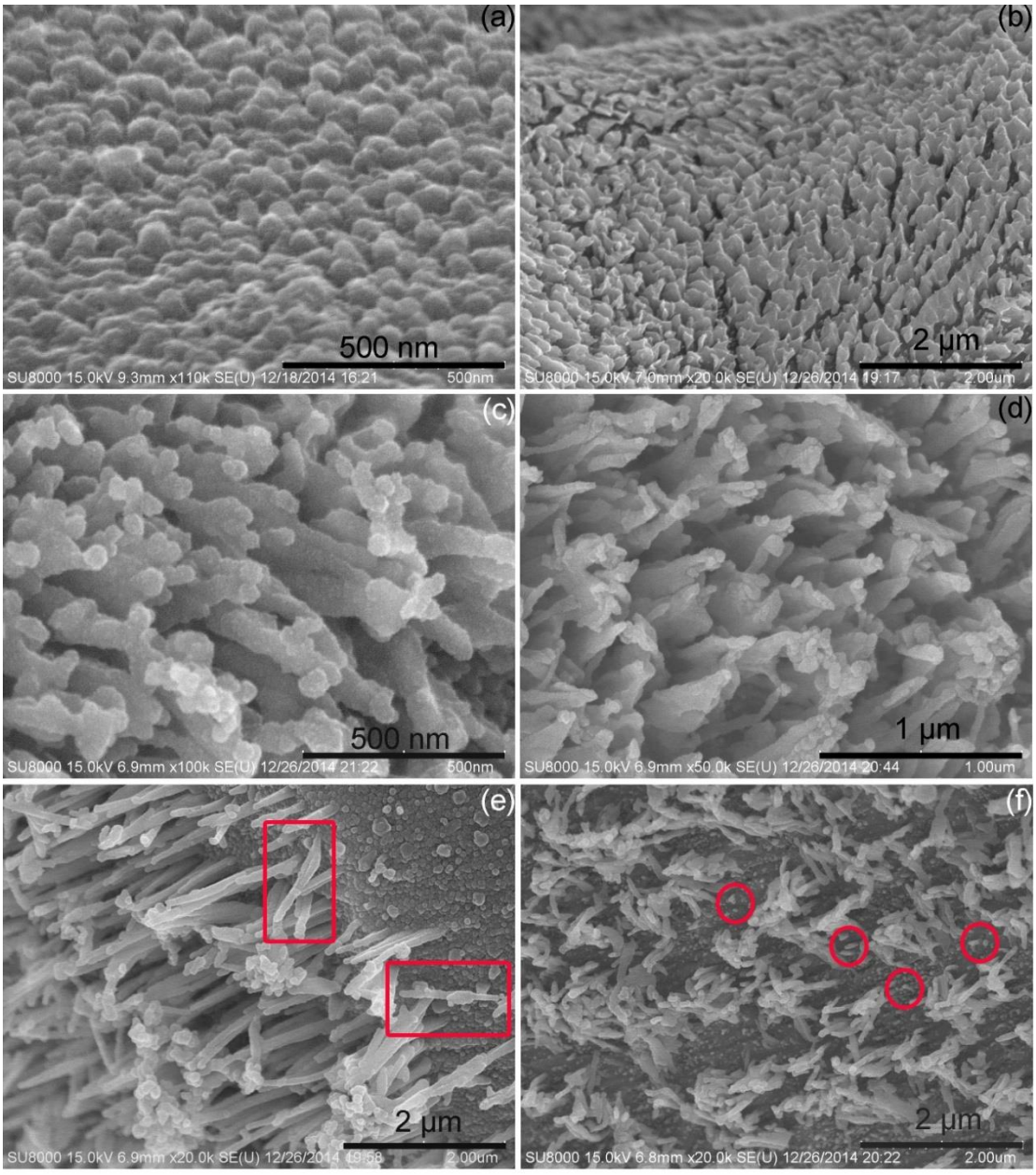


Fig. S5. SEM images of Ti foams treated in HF solution with different times: (a) 30s, (b), 100s, (c) 300s, (d) 500s, (e) 700s, (f) 900s.

These images show the evolution of the Ti alloy surface with etching time in HF solution. Uniform and widespread Ti nanowire arrays can be obtained as the etching time reaches 700 s.

Table S1. BET surface areas of the raw and corroded Ti foam with various time.

| Samples | raw | 30 s | 500 s | 700 s | 900 s |
|---|---|---|---|---|---|
| BET areas ($m^2 g^{-1}$) | 0.39 | 0.42 | 1.35 | 1.81 | 1.74 |

The surface area increases with the corrosion time, and it's about five fold at 700 s (1.81 $m^2 g^{-1}$) compared with the raw sample (0.39 $m^2 g^{-1}$). However, there is a little decrease when the corrosion time rising to 900 s due to the nanowire breakage. Therefore, the etching time for obtaining uniform and widespread Ti nanowire arrays in the present study is set at 700 s.

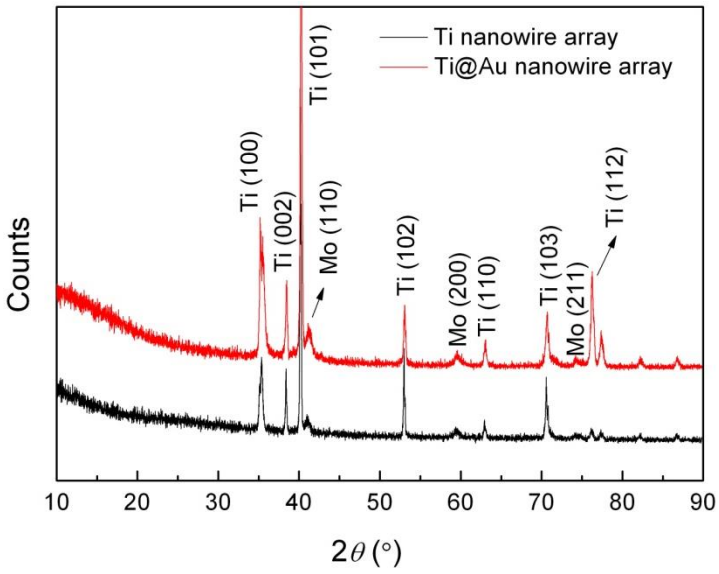


Fig. S6. XRD pattern of Ti foam treated in HF solution for 700s.

Several weak peaks are assigned to Mo metal (JCPDS: 65-7442 *a*=3.147, *b*=3.147, *c*=3.147) are evident. The precipitate of Mo grains on the sample surface causes the Mo diffraction peaks to be clearer when compared to the raw Ti foam (Fig. S2) verifying the proposed mechanism of Ti nanowires generation.

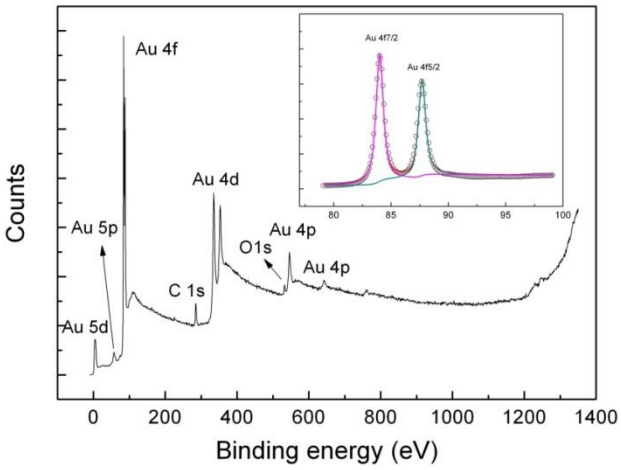


Fig. S7. XPS of as-prepared Ti@Au nanowire arrays. The inset is the high resolution spectra of Au 4f.

Au is the primary element on the array surface, detected from the survey. The high resolution XPS spectra of Au 4f in the inset is characterized by a doublet containing a binding energy of 84.0 eV (Au 4f7/2) and 87.5 eV (Au 4f5/2). The two peaks have a binding energy difference of 3.5 eV and a peak area ratio of 4:3, which corresponds to the characteristics of Au (0).

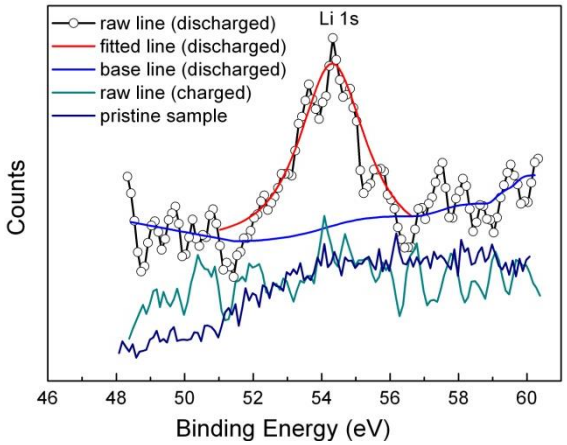


Fig. S8. High resolution XPS spectra of Li 1s from Ti@Aunanowire arrays after the 1st discharge.

Based on the previous result on the discharged sample using the same electrolyte, the peaks (54.3 eV for Li) can be assigned to $Li_2O_2$.

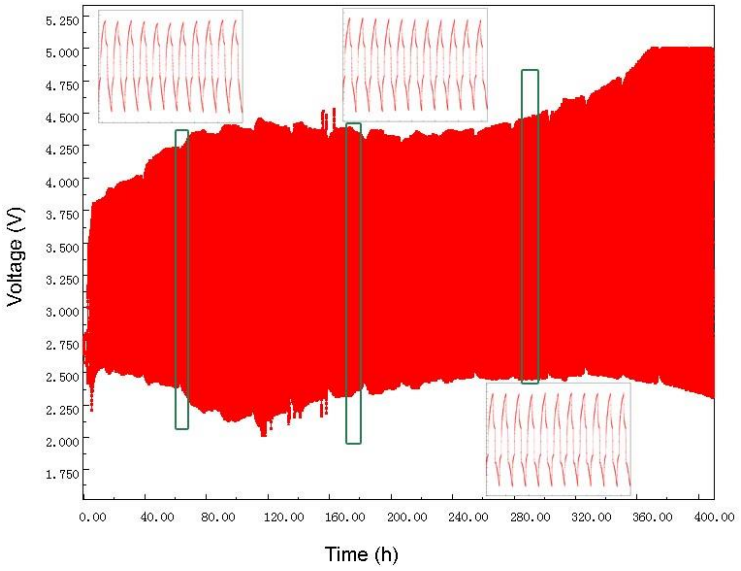


Fig. S9. Momentary curve of voltage evolving with the discharge/charge cycle, insets are actual curves of the 100$^{th}$–110$^{th}$, 300$^{th}$–310$^{th}$, and 500$^{th}$–510$^{th}$ cycles.

The momentary voltage of the battery is dependent on the time but indicates excellent durability in that the battery is maintained for more than 360 h before the end voltages of discharge and charge reach the limiting values (2.0 or 5.0 V).

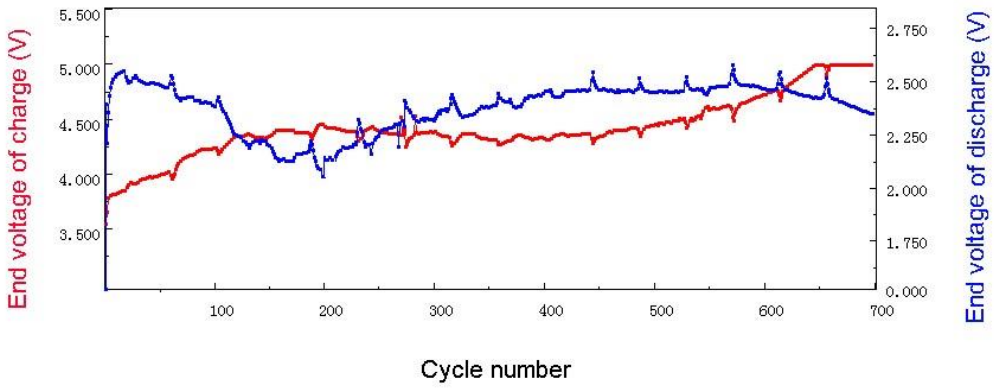


Fig. S10. Curves of discharge/charge end voltage responding to cycle number.

The discharge overpotential grows more slowly than the charge overpotential. Even after the 640$^{th}$ cycle, the end voltage of discharge still is higher than 2.3 V as the charge voltage reaches 5.0 V.

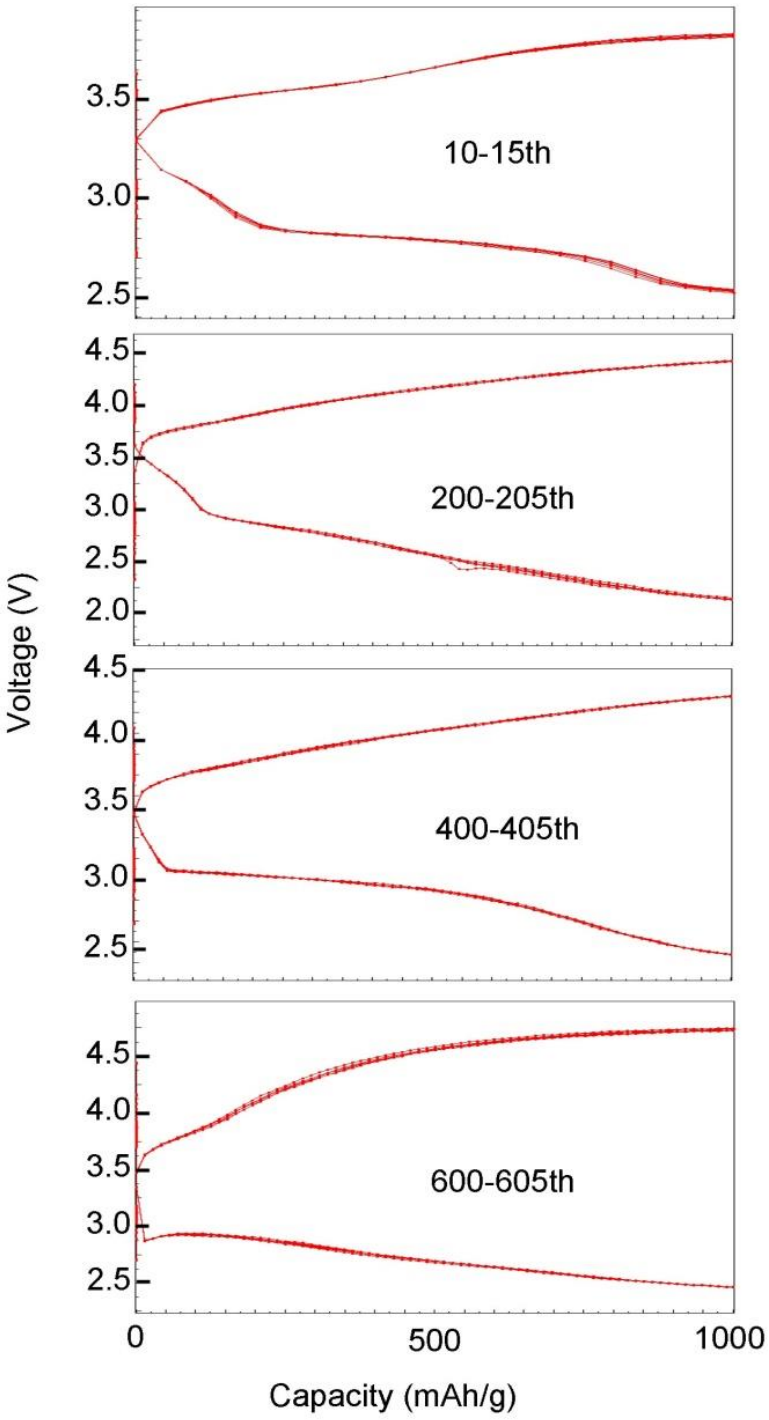


Fig. S11. Discharge/charge curves of the $10^{th}$–$15^{th}$, $200^{th}$–$205^{th}$, $400^{th}$–$405^{th}$, and $600^{th}$–$605^{th}$ cycles.

The oxygen flowing in the battery is seen to have a fluctuation around the $200^{th}$ cycle, resulting in varying overpotential.

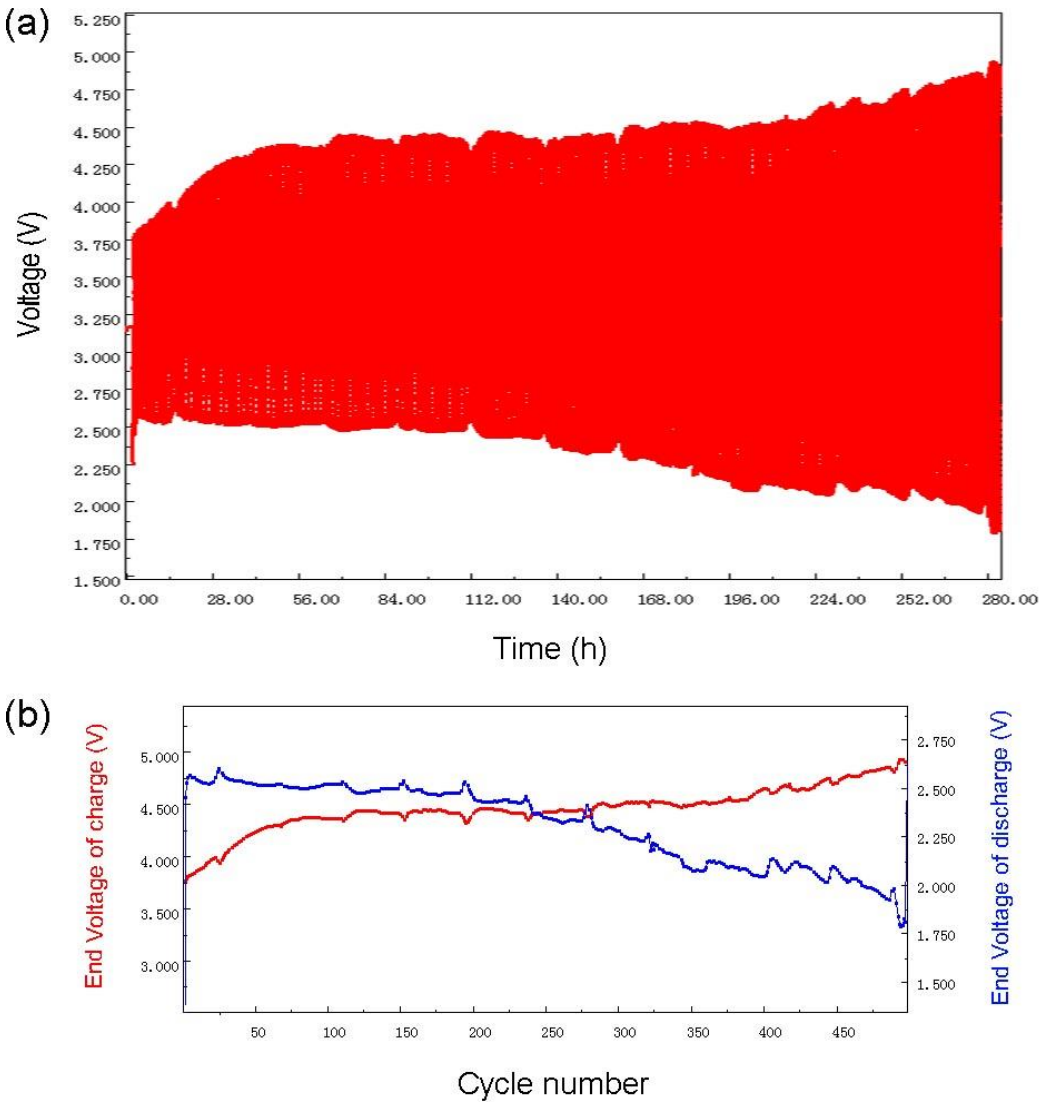


Fig. S12. Cycle performances of a parallel battery carried out at a current density of 5 A $g^{-1}$ within a capacity limitation of 1000 mAh $g^{-1}$: (a) the voltage curve dependent on battery operating time; (b) curves of discharge/charge end voltage responding to cycle number.

Here a parrallel battery battery cycles more than 500 times at a current density of 5 A $g^{-1}$ within a capacity limitation of 1000 mAh $g^{-1}$, demonstrating the good reproducibility of our batteries.

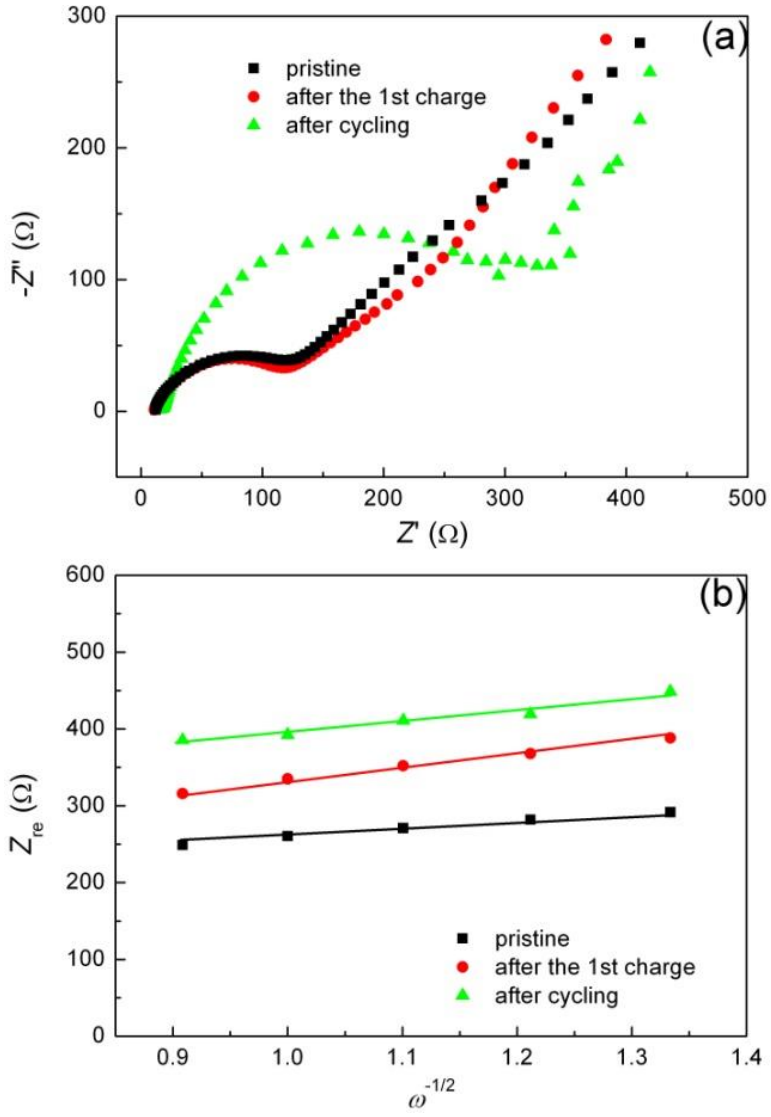


Fig. S13. Impedance study of Ti@Au nanowire arrays at the stages of pristine battery, after the 1st charge and after cycling: (a) Nyquist plots; (b) the relationship between $Z_{re}$ and $\omega^{-1/2}$in the low-frequency region.

Oxygen diffusion kinetics in the cathodes at different stages was examined by comparing the diffusion coefficients, which were calculated according to the following equation:

$$\sigma = \left[\frac{RT}{\sqrt{2}n^2F^2AC_{O_2}}\right]\frac{1}{\sqrt{D_{O_2}}}, \qquad \text{(Equation S1)}$$

and converted to

$$D = \frac{R^2T^2}{2n^4F^4A^2\sigma^2C_{O2}^2}, \quad \text{(Equation S2)}$$

where $n$ is the number of electrons per-molecule during the $O_2$ reaction, $A$ is the surface area of the anode, $D$ is the diffusion coefficient of $O_2$, $R$ is the gas constant, $T$ is the absolute temperature, $F$ is the Faraday constant, $C$ is the concentration of lithium ions, and $\sigma$ is the Warburg factor which has a relationship with $Z_{re}$:

$$Z_{re} = R_D + R_L + \sigma\omega^{-1/2}, \quad \text{(Equation S3)}$$

where $Z_{re}$ is the real part of the resistance in the low frequency region, $\omega$ is the corresponding frequency. Fig. S13b shows the relationship between $Z_{re}$ and the square root of frequency ($\omega^{-1/2}$) in the low-frequency region. The ratio of diffusion coefficients of $O_2$ in the pristine cathode, after the 1$^{st}$ charge and after cycling is 10:3.6:4.7. Obviously, the diffusion coefficients of $O_2$ at the three stages are at a similar order of magnitude.